

# A scalable network for simultaneous pairwise quantum key distribution via entanglement-based time-bin coding

L. Bialowons, E. Fitzke, M. Tippmann, O. Nikiforov, and T. Walther\*

*Institute for Applied Physics, Technische Universität Darmstadt,  
Schlossgartenstraße 7, 64289 Darmstadt, Germany*

F. Wissel and M. Gunkel

*Deutsche Telekom Technik GmbH, Heinrich-Hertz-Straße 3-7, 64295 Darmstadt, Germany*

(Dated: December 22, 2021)

We present a star shaped optical fiber network for simultaneous quantum key distribution (QKD). Our QKD system is the first entanglement-based time-bin coding network of four participants. We demonstrate simultaneous bipartite key exchange between any possible combination of receivers for distances of more than 75 km. As the key distribution is insensitive to polarization instabilities in the network, precise temperature control of the imbalanced interferometers in the source and receivers is sufficient to provide stable quantum bit error rates (QBER). In fact, the QBER is used to stabilize the phase in the interferometers by small temperature adjustments. We demonstrate raw key rates of  $(29 \pm 3)$  bits $^{-1}$  and QBERs of 2.63 % over a total fiber length of 60.55 km with high stability. Moreover, our scheme is compatible to multiplexing approaches. Thus, the all-fiber system enables key distribution networks using deployed fibers even under challenging environmental conditions making it suitable for, e.g., securing communication infrastructure and establishing robust metropolitan-scale QKD networks. In particular, the network can be readily extended to more than 100 participants with only slight modifications.

## I. INTRODUCTION

The advent of quantum computers poses a risk for classical public-key cryptography [1–3]. One possible solution to this problem is quantum key distribution which uses quantum signals to share cryptographic keys between users [4–6]. To date, a variety of QKD protocols, setups and testing links have been implemented and the achievable key rates and distances have continuously been increased [6]. One major research direction has been to demonstrate long-distance QKD. Key exchange over hundreds of kilometers of optical fiber [7–10] as well as with satellite-based links spanning thousands of kilometers [11, 12] have been demonstrated. Another focus of current research is the implementation of multi-user QKD networks often based on trusted nodes, i.e. relay stations set up between the network users that have full knowledge of the key.

Currently, the largest of such networks is the Chinese QKD network connecting Beijing and Shanghai via a 2000 km long quantum backbone link that includes multiple metropolitan-area QKD networks [13]. The big drawback of this trusted-node approach is that it is not applicable in situations where the users do not trust the network provider operating the central node. Alternative approaches to set up QKD networks not requiring trust in the central node can be realized by measurement-device-independent protocols or with entanglement-based protocols [6, 14–16].

Setups using dense wavelength division multiplexing (DWDM) for the distribution of polarization-entangled photons via optical fibers have been realized for photons generated by spontaneous parametric down-conversion (SPDC)

in periodically poled fibers [17] or crystals [18–20]. Distribution of polarization-entangled photon pairs has been successfully implemented over submarine fibers [21, 22] and was the basis for a demonstration of a city-scale QKD network with eight users based on polarization coding [15].

QKD protocols using photon polarization require active polarization control because the birefringence in single-mode fibers can change over time, leading to large fluctuations of the initial polarization state. For fiber deployed underground, the polarization change in short fibers can be on a time scale of hours to days [23]. However, substantially faster polarization changes have been observed in urban areas [24]. In ref. 25, polarization fluctuations and their impact on QKD systems were systematically characterized and the required polarization tracking speed was measured to be on the order of multiple rad s $^{-1}$  for inter-city and aerial links. Estimates show that polarization adjustments on a millisecond timescale are necessary for stable operation of a 68 km long aerial fiber QKD link [26]. Compensation schemes for the stabilization of the polarization drift have been proposed [27–29], but considerably increase the complexity of QKD setups. Schemes re-adjusting the polarization based on the quantum bit error rate (QBER) can only compensate sufficiently slow polarization changes. Depending on the key rate, some time is required in order to accumulate sufficiently many bits so that the QBER can be reliably estimated. Hence, QBER-based polarization stabilization may become infeasible for long transmissions distances with low key rates and fast polarization changes.

In contrast to polarization-based QKD, protocols using the phase and arrival time of photons to encode qubits are very robust and independent of polarization changes. However, for phase-coding protocols, the critical parts of the setup that need stabilization are the interferometers located in a controlled environment at the locations of the communication partners.

\* thomas.walther@physik.tu-darmstadt.de

Achieving stable operation is independent of environmental influences on the transmission link. Stable key exchange is therefore even possible under relatively harsh environmental conditions.

In this paper, we implement a time-bin based variant of the BBM92 protocol [30–32] in a four-party quantum network. We use a wide SPDC spectrum and DWDM in the optical C-band to demonstrate simultaneous key exchange between the four participants employing a single photon source. Our setup is readily scalable to 34 network users and compatible with DWDM multiplexing schemes that were previously used to establish QKD networks [15, 33]. With slight modifications, it can even scale up to 102 participants.

## II. QKD PROTOCOL

In the original implementation of the protocol, a photon pair source is placed between two QKD users Alice and Bob [32]. Each user holds a receiver module consisting of an imbalanced interferometer with two single-photon detectors at the outputs (cf. Fig. 1(a)). The basic idea of the protocol is as follows: In the photon pair source, pump pulses are sent through an imbalanced interferometer. The pulse duration is chosen to be shorter than the time delay, so that each pump pulse is split into a pair of non-interfering pulses. These pulses are then used to pump a nonlinear process such as SPDC or spontaneous four-wave mixing to produce entangled photon pairs. The pulse energy is chosen such that the mean number of photon pairs per pulse  $\mu \ll 1$ , i.e. the probability that a pulse generates more than one photon pair is low.

Alice and Bob each receive one of the photons and detect it in one of three different time bins, as seen in Fig. 1(b). If the first laser pulse produces a photon pair, Alice and Bob detect their photons in the early or central time bin. Photons generated by the late laser pulse are detected in the central or late time bin. For detections in the early or late time bin Alice and Bob note down a 0 or 1, respectively. Detections in the central time bin are noted down as 0 or 1 depending on which of the two detectors clicked. When the time delays of all three interferometers are matched, two-photon Franson interference [34] leads to detection in correlated outputs for photons arriving in the central time bin.

In an ideal setup with perfectly indistinguishable interferometers, the probability for detection at two correlated outputs is [32, 35]

$$P_{A_i, B_j}(\alpha, \beta, \phi) = \frac{1}{4} (1 + (-1)^{i+j} \cos(\alpha + \beta - \phi)) \quad (1)$$

with detector labels  $i, j \in 0, 1$ . When the phases in the interferometers of Alice ( $\alpha$ ), Bob ( $\beta$ ) and the source ( $\phi$ ) are aligned to  $\alpha + \beta - \phi = 2\pi n$  with  $n \in \mathbb{Z}$ , Alice and Bob will always obtain the same bit values. In this protocol, the two orthogonal bases required for QKD are the time basis consisting of measurements in the early and late time bin and the phase basis consisting of measurements of the detector number in the central time bin. In the key sifting step, Alice and Bob announce in which basis they measured the photon. If both detected a

photon in the same basis, they append the corresponding bit value to the key. All events measured in different bases are discarded.

Distribution of such time-bin entangled photons was realized over 50 km [35] and 300 km [36] and QKD using this scheme was implemented in a field test between two participants over 100 km [37]. Distributing time- and wavelength-entangled photons with DWDM was previously demonstrated using photon sources based on spontaneous four-wave mixing in optical fibers [33] and silicon waveguides [38].

We extend wavelength-multiplexed entanglement distribution to a multi-user QKD network.

## III. SETUP

Wavelength demultiplexing can distribute photon pairs at different wavelengths to more than two participants, which we employ to extend the key distribution scheme to a star-shaped multi-user network with the photon pair source at the center (Fig. 1(c)). In our experimental setup, depicted in Fig. 2(a), we connect an arrayed waveguide grating (AWG) for wavelength-division demultiplexing to a photon pair source to realize this network structure.

In contrast to the idealized setup shown in Fig. 1(a), we use Michelson interferometers with Faraday mirrors instead of Mach-Zehnder interferometers in order to remove the polarization dependence from our setup (cf. Fig. 2(b)) [39–41]. Therefore, our setup does not require polarization stabilization. We set up four identical receiver modules for the four participants Alice, Bob, Charlie and Diana to demonstrate simultaneous pairwise key exchange. The receiver modules are connected to the AWG via fiber spools of single-mode fiber with an attenuation of around  $0.22 \text{ dB km}^{-1}$  typical for field deployed optical fibers.

The all-fiber design makes our setup compact and robust. As pointed out earlier, phase stability of the interferometers is critical. Our phase stabilization is based on the precise temperature control of the interferometer temperatures. Due to the high temperature stability of approximately  $0.5 \text{ mK}$ , the phase adjustment can be solely based on the estimated QBER. In the following, we will briefly discuss the experimental details.

### A. Photon Source

Photon pairs are created via a multi-stage process. The primary light source is a continuous-wave laser (model Clarity, Wavelength References) frequency locked to 1550.52 nm, i.e. between the channels C33 and C34 of the ITU DWDM grid. A  $\text{LiNbO}_3$  amplitude modulator (iXblue, 10 GHz) shapes pulses with a repetition rate of 219.78 MHz and a width of about 300 ps. The repetition time of 4.55 ns is chosen such that there is no overlap between the time bins that belong to two successive pump pulses (Fig. 3). The pulses are amplified to an energy of up to 90 pJ by an in-house-built erbium-doped fiber amplifier (EDFA) and are passed through the source's Michelson interferometer. A fiber-coupled PPLN

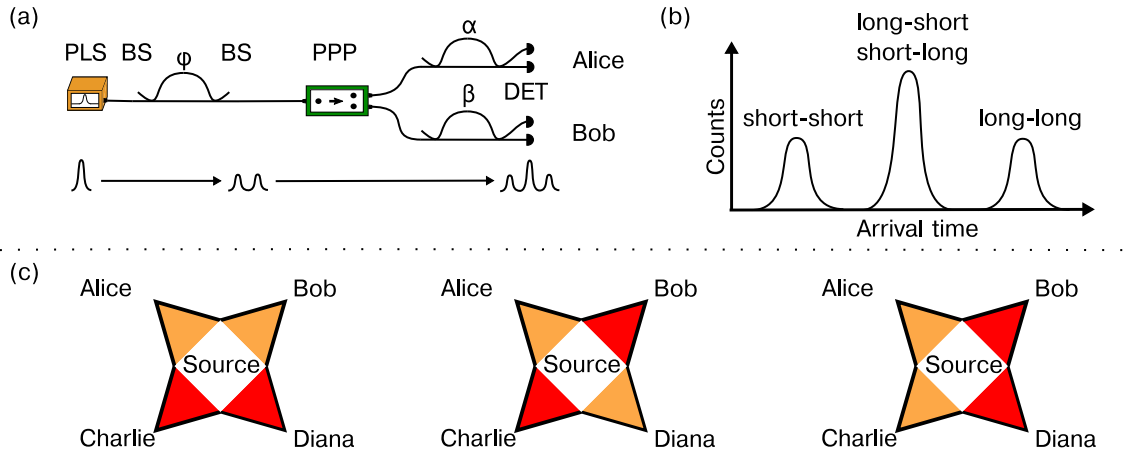


FIG. 1. (a) Scheme for time-bin entanglement quantum key distribution. PLS: Pulsed laser source, BS: 50:50 beam splitter, PPP: Photon pair production, DET: Single-photon detector. The symbols  $\phi$ ,  $\alpha$  and  $\beta$  indicate the phase delay of the interferometers. (b) Arrival time histogram at one of the detectors. Depending on the combination of long and short paths taken in the pump and receiver interferometers, the photons arrive in one of three time bins. Clicks in the satellite and central peaks yield detections in the time basis and phase basis, respectively. (c) Different configurations of a 4-participant star-shaped network. Pairwise communication between participants marked in the same color is possible for all combinations of Alice, Bob, Charlie and Diana. Pairs marked with different colors can exchange keys simultaneously.

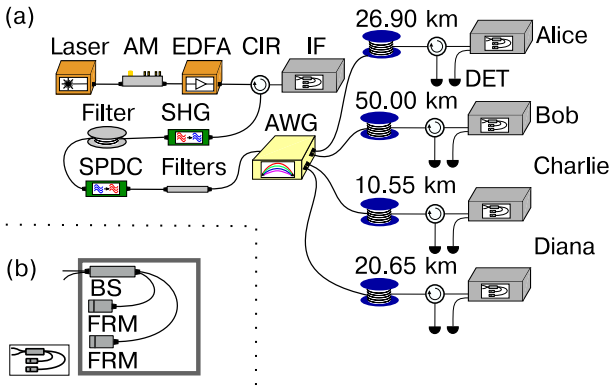


FIG. 2. (a) Setup for time-bin entanglement quantum key distribution with four participants. AM: Amplitude modulator, EDFA: Erbium-doped fiber amplifier, CIR: Circulator, IF: Interferometer, SHG: Second harmonic generation, SPDC: Spontaneous parametric down-conversion, AWG: Arrayed waveguide grating, DET: Single-photon detector (b) Setup of the interferometers. BS: 50:50 beam splitter, FRM: Faraday rotator mirror. All interferometers are placed in temperature-stabilized boxes.

crystal (NTT Electronics) converts the wavelength to 775 nm via second harmonic generation (SHG). Several meters of tightly wound single-mode fiber are used to filter out remaining light around 1550 nm. A second PPLN crystal of the same type is used to generate energy-time entangled photon pairs in a type-0 SPDC process [42, 43]. The SPDC frequency spectrum is symmetric around the center frequency with approximately 9.3 THz (75 nm) FWHM. High-pass filters remove the remaining 775 nm-light.

After passing a C-band filter transmitting all photons within a range of  $\pm 2.55$  THz around our center frequency, the photons are distributed to the receivers by a standard telecommu-

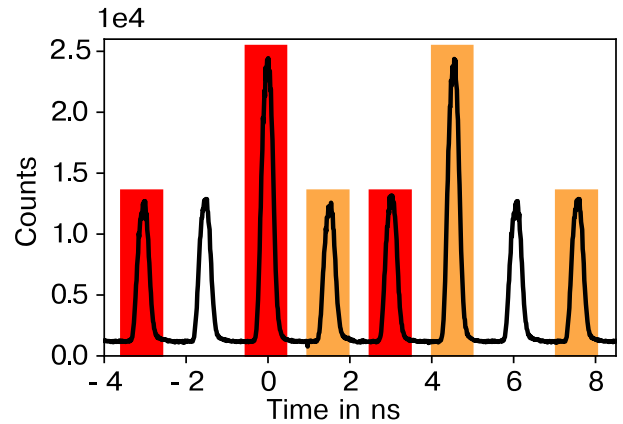


FIG. 3. Histogram of detected events at one of Charlie's detectors with time bins marked in orange and red. Events located in time bins of the same color originate from the same pump pulse. Even though the time separation between the outer time bins is larger than the repetition time of 4.55 ns (corresponding to 219.78 MHz), there is no overlap between time bins due to interleaving. The data was acquired during a 90 second long measurement over 10.55 km of fiber.

nication AWG with 100 GHz channel spacing. The C-band filter removes unwanted photons that originate from adjacent diffraction orders of the AWG. In order to set up a key exchange between a pair of participants, their fibers are connected to a pair of AWG channels that is symmetric around the center frequency and within the C-band filter's pass band. The number of available channels is limited by the lowest channel number of our AWG, which is C17. Therefore, 17 symmetric pairs of 100-GHz channels from C17 to C50 are available for key exchange resulting in 34 possible participants in the network.

## B. Receiver interferometers

The interferometers in the source and the receiver should be as similar as possible. Furthermore, the phase stability between the interferometers is of utmost importance. Therefore, we paid special attention to the design of the interferometers.

The Michelson-type interferometers feature path length differences of 3.03 ns. They consist of polarization-independent 50:50 beam splitters and Faraday rotator mirrors eliminating the sensitivity to birefringence in the interferometer arms [39–41] and enabling two-photon interference independent of the polarization state of incoming photons. The path combinations long-short and short-long in the pump and receiver interferometers need to be almost indistinguishable in order to achieve a sufficient two-photon interference visibility. Therefore, the differences between the time delays of the interferometers must be much smaller than the coherence lengths of the photon pairs. We carefully manufactured our interferometers to keep the deviation of path length differences below 200  $\mu\text{m}$ . After splicing of the fiber components, the path lengths of the interferometers were fine tuned. Each interferometer is enclosed by a box to shield it from environmental temperature fluctuations. The box temperature can be adjusted with thermo-electric elements driven by digitally controllable temperature controllers developed in-house. The sensitivity of the interferometer phase to temperature changes is in the range of  $0.033\pi\text{ mK}^{-1}$  to  $0.045\pi\text{ mK}^{-1}$ . The box temperature can be adjusted with a precision of 0.5 mK.

Chromatic dispersion in fibers broadens the peaks in the arrival time histogram. On the one hand, if the time delay in the interferometers is chosen too small, chromatic dispersion will lead to overlapping peaks in the photon arrival time histograms and thus to an increased QBER for transmission over long fibers. On the other hand, a large time delay limits the pulse repetition rate. In order to be able to test the system with long fibers without dispersion compensation, we chose a time delay of around 3 ns. For the fiber lengths used in this paper, the broadening from chromatic dispersion is small enough so that we could interleave consecutive repetition cycles in order to double the repetition rate (cf. Fig. 3).

## C. Data acquisition and phase calibration

The photons are detected by avalanche single-photon detectors (ID Quantique ID220) with a timing jitter of about 250 ps. All detectors are set to 20 % quantum efficiency with a dead time of 10  $\mu\text{s}$ . Timestamps are recorded by time taggers (ID Quantique ID900) with 13 ps resolution synchronized to the pulsed laser source.

We have extensively automated the setup operation and data acquisition. Data acquisition is split into 90 second long runs with approximately 6 second long intermissions for qubit evaluation. During the startup phase, differences in arrival time of the photons resulting from different fiber lengths are calculated automatically. The calculation typically takes around 15 seconds and the results are reused for all subsequent runs.

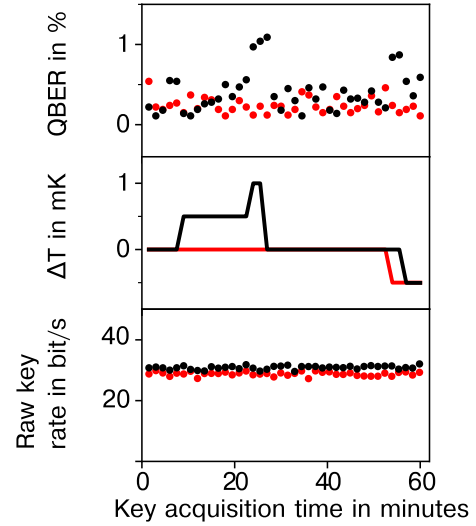


FIG. 4. A simultaneous key exchange for Alice/Diana (red) and Charlie/Bob (black) without fiber spools and with  $\mu$  below  $1 \times 10^{-3}$  demonstrating low quantum bit error rates (QBER).  $\Delta T$  denotes the temperature adjustments made at Alice's and Bob's receiver to minimize the error rate. Each data point was obtained from one run of 90 s. The average QBER was 0.24 % for Alice/Diana and 0.41 % for Charlie/Bob.

Our setup requires clock synchronization between the photon source and the time taggers. Temperature changes of the spooled fibers can cause an arrival time drift, which is compensated automatically after each run through analysis of the photon arrival times at each detector. In addition to the arrival time calibration, the interferometer phases are automatically calibrated such that a minimal QBER is reached. The whole startup takes at most 45 minutes and can be completed significantly faster if the interferometers are already aligned.

After the startup, key exchange can commence. In each 6 second-long intermission, the QBER is estimated in order to detect interferometer phase drifts. The box temperatures of all participants can be adjusted automatically every three minutes in order to keep the QBER as low as possible.

## IV. RESULTS

The QBER during key exchange with our setup strongly depends on the mean number of photon pairs per pulse  $\mu$ . For values of  $\mu$  below  $1 \times 10^{-3}$ , low QBERs are expected because the emission of multiple photon pairs per pulse becomes highly unlikely. In order to assess the achievable quality of the correlations in the phase basis, measurements with an average SHG power of 0.75  $\mu\text{W}$  were performed without additional fiber spools between the source and the receiver. Fig. 4 shows a one-hour long key exchange for such low values of  $\mu$ . An average QBER of 0.24 % was reached for Alice/Diana and of 0.41 % for Charlie/Bob. The QBER for Charlie/Bob shows maxima around 28 minutes and 55 minutes which were caused by phase drifts in the respective interferometers during the measurement. However, the automatic phase calibration

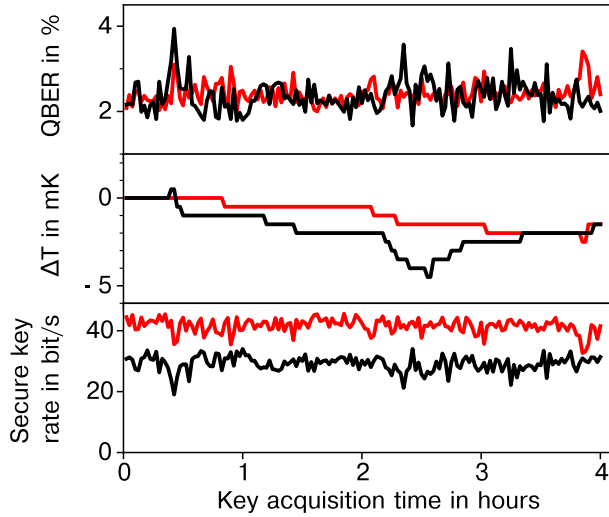


FIG. 5. Estimated secure key rates and QBER for simultaneous key exchange over fiber spools with a total length of 47.55 km for Alice/Diana (red) and 60.55 km for Charlie/Bob (black) with a  $\mu$  in the range of 0.03.  $\Delta T$  denotes the temperature adjustments made at Alice's and Bob's receiver interferometers. Each data point represents one 90 second long run.

compensated for the drift and the QBER quickly returned to lower values. Since the QBER is a symmetric error function yielding no information regarding the direction of the phase drift, the algorithm occasionally adjusts the temperature in the wrong direction, as seen for the peak at 28 minutes. However, the algorithm quickly recognized the wrong decision and corrected it automatically. Between 30 minutes and 50 minutes, no temperature adjustments were necessary for either party. Key exchange between Alice/Diana did not require any temperature adjustments for more than 50 minutes. The very low error rates show that the losses and time delays in the arms of our interferometers are well matched.

The reliability of our phase stabilization algorithm was estimated in a long-term measurement over several hours of continuous operation. For these measurements, the average number of photons per pulse  $\mu$  created in the frequency range of one channel pair was increased to be in the range of 0.03 corresponding to an average SHG pump power of 30  $\mu$ W. A four-hour long key exchange between the pairs Alice/Diana and Charlie/Bob with an average QBER of 2.41 % for Alice/Bob and 2.36 % for Charlie/Diana is shown in Fig. 5. As before, the automatic phase stabilization algorithm adjusts the interferometer temperatures such that the error rate stays at a minimum. Even though the temperature of the interferometers can be adjusted every three minutes, the error rates remained stable over periods much longer than that demonstrating an excellent phase stability.

The sum of the fiber lengths Source-Alice and Source-Diana, i.e. the effective key transmission distance, was 47.55 km achieving an average raw key rate of 70  $\text{bit s}^{-1}$ . Between Charlie and Bob the effective distance was 60.55 km (cf. Fig. 1(a)) with a raw key rate of 49  $\text{bit s}^{-1}$ . Assuming error reconciliation based on low-density parity-

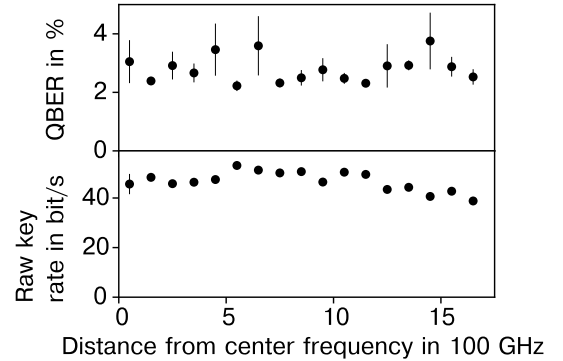


FIG. 6. Quantum bit error rate (QBER) and raw key rate for key exchange between Charlie and Bob over 60.55 km of fiber for different AWG channel pairs symmetric around our center frequency. Each data point was averaged over 8 consecutive 90 second runs. The error bars represent the standard deviation of the results for each channel.

check codes, we estimated the secure key rates  $r_{\text{secure}}$  which can be calculated from the raw key rate  $r_{\text{raw}}$ , the QBER  $q$  and the reconciliation efficiency  $f$  (cf. ref. 44):

$$r_{\text{secure}} = r_{\text{raw}} (1 - (1 + f) (-q \log_2(q) - (1 - q) \log_2(1 - q))). \quad (2)$$

Using a conservative estimate for the reconciliation efficiency of  $f = 1.5$  (cf. ref. 44), we estimated the average secure key rate as  $(42 \pm 3) \text{ bits s}^{-1}$  for Alice/Diana over 47.55 km and  $(29 \pm 3) \text{ bits s}^{-1}$  for Charlie/Bob over 60.55 km.

One main advantage of our system is the scalability of the photon source with respect to the number of users. In order to demonstrate that all 34 available channels are usable for key exchange, we connected the pair Charlie/Bob over a distance of 60.55 km of fiber and measured the QKD performance with each of the 17 available channel pairs (cf. Fig. 6). All channel pairs in the pass band of the C-band filter offer a similar performance. Thus, with a channel spacing of 100 GHz of the AWG, we conclude that 34 participants can be connected to our source simultaneously.

In order to assess the capabilities of our system over distances typical for metropolitan quantum networks, the performance of the network was investigated by connecting the AWG and the receivers with fibers of different lengths for each participant (cf. Fig. 2(a)). In this case, the communication between different pairs of participants is set up by reconfiguring the AWG connections and recalibrating the receiver interferometer phases. This is done via the same startup procedure described above. We tested all possible network configurations (cf. Fig. 1(c)) and demonstrated successful key exchange between all combinations of all four participants, as shown in Fig. 7. The results were obtained with the same mean photon pair number per pulse  $\mu$  for all combinations. Hence, key exchanges over total distances between 31.2 km and 76.9 km were achieved.

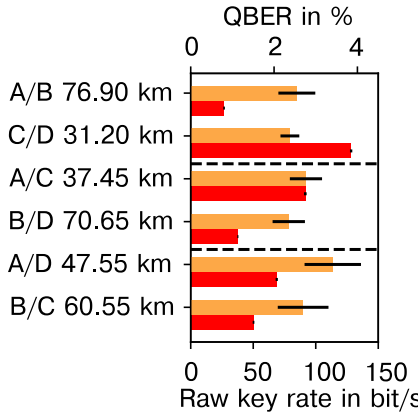


FIG. 7. QBER (orange) and raw key rates (red) for all combinations of the four participants Alice, Bob, Charlie and Diana (A,B,C,D) over different fiber lengths. Fiber spools were assigned as shown in Fig. 2(a). The data was obtained during three 20-run measurements (A/B C/D; A/C B/D; A/D B/C) via simultaneous pairwise key exchange. The error bars represent the standard deviation of the results for each combination.

## V. DISCUSSION AND OUTLOOK

Our QKD system proved to be able to distribute quantum keys between any two pairs of participants simultaneously without requiring a trusted node. The high stability of the QBER is reflected in the low standard deviation of the secure key rates. Our results are a considerable improvement over the stability achieved recently by a comparable multi-user network using polarization entanglement [15], despite much longer transmission distances in our network. We attribute this increased stability to the fact that our protocol is insensitive to environmental effects impairing the polarization stability of the transmission fiber. For the same reason, we expect that our system, when used in the field with deployed fiber can achieve a stability that is comparable to the performance demonstrated with fiber spools. This will enable QKD even in challenging environmental conditions, such as transmission via aerial fiber or through densely populated urban areas.

Furthermore, the 17 channel pairs we used here only span a frequency range of 3.4 THz. If the full width of our C-band filter was used, QKD would be possible for ITU channels 8 to 59. Thus, up to 102 participants could be connected to our photon source for simultaneous pairwise key exchange with a suitable 50 GHz AWG.

Of course, pairwise communication is only one application scenario for multi-user networks. Approaches based on wavelength- and time-division multiplexing are compatible with our setup. Wavelength-division multiplexing schemes as presented in ref. 15 and 20 could be used to implement fully-connected networks with our setup, since they also use type-0 SPDC photon sources. Moreover, in combination with active or passive time multiplexing, networks with participants grouped in fully connected sub-networks can be realized [38, 45]. An alternative to such schemes with a fixed

channel allocation is to allocate the bandwidth dynamically based on key rate demand with a wavelength-selective switch as demonstrated for entanglement-based QKD [46].

The key rates of our setup are currently limited by the repetition rate of our source and the detection efficiency and dead time of the APDs employed. For example, commercial superconducting nanowire single-photon detectors (SNSPD) can reach polarization-independent efficiencies greater than 70 % with full recovery times around 60 ns (e.g. IDQ ID281) [47]. Using such detectors could increase the key rate by a factor of at least 12.3, solely due to the improvement of detector efficiency from 20 % to 70 %. In addition, the limit on the key rate imposed by our detector dead time of 10  $\mu$ s can be overcome with SNSPDs due to their short recovery time. An increase of the repetition rate for a constant mean photon pair number per pulse  $\mu$  will lead to an almost proportional increase of key rates when the detector dead times are shorter than the time bin width. The width of the time bins could be reduced further by using shorter pump pulses, dispersion compensation and a detection setup with less jitter.

Assuming that a width of 95 ps per time bin is feasible, the repetition rate could be increased by a factor of 16 to approximately 3.5 GHz. At this repetition rate, 32 pulses interleave without overlap between time bins, which generalizes the method shown in Fig. 3.

The increase in efficiency and repetition rate will result in an overall improvement of the raw key rate by a factor of approximately 197 compared to the data presented here, i.e. raw key rates above 9 kbit/s<sup>-1</sup> over a distance of 60 km of standard telecommunication fiber are feasible. While our setup in its current configuration is already suitable for communication over metropolitan-area distances, SNSPDs and higher repetition rates can be used to increase the transmission distances significantly beyond 100 km.

## VI. CONCLUSION

We presented an all-fiber entanglement-based QKD system enabling simultaneous key distribution between any two pairs of participants by employing wavelength division multiplexing. Simultaneous key exchange was demonstrated over distances between 31.2 km and 76.9 km. The quantum bit error rate (QBER) is automatically optimized by aligning the phase of the receiver interferometers via temperature adjustments.

Our system is readily scalable to simultaneously provide 17 pairs of participants with keys. With suitable 50 GHz demultiplexing, the size of our network can be extended to more than 100 participants. We obtained raw key rates of  $(29 \pm 3)$  bits/s<sup>-1</sup> and QBERs of 2.63 % over a total fiber length of 60.55 km with high stability.

Time- and wavelength-division multiplexing schemes demonstrated with polarization-based entanglement protocols can be applied to our scheme as well. However, in contrast to networks using polarization encoding, our setup is resistant to environmental disturbances deteriorating the polarization in the transmission fiber. This allows for a considerable improvement in terms of the stability of secure key rates due to

the reduced QBER. These advantages of time-bin coding can be readily combined with wavelength division multiplexing for robust metropolitan-scale networks.

## ACKNOWLEDGEMENT

This research has been funded by the Deutsche Forschungsgemeinschaft (DFG, German Research Foundation) – SFB 1119 – 236615297

We thank Paul Wagner from Deutsche Telekom Technik GmbH for lending us the AWG and fiber spools.

## DATA AVAILABILITY STATEMENT

The data that support the findings of this study are available from the corresponding author upon reasonable request.

---

[1] R. A. Grimes, *Cryptography Apocalypse - Preparing for the Day When Quantum Computing Breaks Today's Crypto* (John Wiley & Sons, New York, 2019).

[2] D. Cheung, D. Maslov, J. Mathew, and D. K. Pradhan, On the design and optimization of a quantum polynomial-time attack on elliptic curve cryptography, in *Theory of Quantum Computation, Communication, and Cryptography*, edited by Y. Kawano and M. Mosca (Springer Berlin Heidelberg, Berlin, Heidelberg, 2008) pp. 96–104.

[3] E. Gerjuoy, Shor's factoring algorithm and modern cryptography: an illustration of the capabilities inherent in quantum computers, *American Journal of Physics* **73**, 521 (2005), <https://doi.org/10.1119/1.1891170>.

[4] N. Gisin, G. Ribordy, W. Tittel, and H. Zbinden, Quantum cryptography, *Rev. Mod. Phys.* **74**, 145 (2002).

[5] V. Scarani, H. Bechmann-Pasquinucci, N. J. Cerf, M. Dušek, N. Lütkenhaus, and M. Peev, The security of practical quantum key distribution, *Rev. Mod. Phys.* **81**, 1301 (2009).

[6] F. Xu, X. Ma, Q. Zhang, H.-K. Lo, and J.-W. Pan, Secure quantum key distribution with realistic devices, *Rev. Mod. Phys.* **92**, 025002 (2020).

[7] M. Pittaluga, M. Minder, M. Lucamarini, M. Sanzaro, R. I. Woodward, M.-J. Li, Z. Yuan, and A. J. Shields, 600-km repeater-like quantum communications with dual-band stabilization, *Nature Photonics* **15**, 530 (2021).

[8] J.-P. Chen, C. Zhang, Y. Liu, C. Jiang, W. Zhang, X.-L. Hu, J.-Y. Guan, Z.-W. Yu, H. Xu, J. Lin, M.-J. Li, H. Chen, H. Li, L. You, Z. Wang, X.-B. Wang, Q. Zhang, and J.-W. Pan, Sending-or-not-sending with independent lasers: Secure twin-field quantum key distribution over 509 km, *Phys. Rev. Lett.* **124**, 070501 (2020).

[9] J.-P. Chen, C. Zhang, Y. Liu, C. Jiang, W.-J. Zhang, Z.-Y. Han, S.-Z. Ma, X.-L. Hu, Y.-H. Li, H. Liu, F. Zhou, H.-F. Jiang, T.-Y. Chen, H. Li, L.-X. You, Z. Wang, X.-B. Wang, Q. Zhang, and J.-W. Pan, Twin-field quantum key distribution over a 511 km optical fibre linking two distant metropolitan areas, *Nature Photonics* **15**, 570 (2021).

[10] A. Boaron, G. Boso, D. Rusca, C. Vulliez, C. Autelbert, M. Caloz, M. Perrenoud, G. Gras, F. Bussières, M.-J. Li, D. Nolan, A. Martin, and H. Zbinden, Secure quantum key distribution over 421 km of optical fiber, *Phys. Rev. Lett.* **121**, 190502 (2018).

[11] J. Yin, Y. Cao, Y.-H. Li, S.-K. Liao, L. Zhang, J.-G. Ren, W.-Q. Cai, W.-Y. Liu, B. Li, H. Dai, G.-B. Li, Q.-M. Lu, Y.-H. Gong, Y. Xu, S.-L. Li, F.-Z. Li, Y.-Y. Yin, Z.-Q. Jiang, M. Li, J.-J. Jia, G. Ren, D. He, Y.-L. Zhou, X.-X. Zhang, N. Wang, X. Chang, Z.-C. Zhu, N.-L. Liu, Y.-A. Chen, C.-Y. Lu, R. Shu, C.-Z. Peng, J.-Y. Wang, and J.-W. Pan, Satellite-based entanglement distribution over 1200 kilometers, *Science* **356**, 1140 (2017).

[12] S.-K. Liao, W.-Q. Cai, J. Handsteiner, B. Liu, J. Yin, L. Zhang, D. Rauch, M. Fink, J.-G. Ren, W.-Y. Liu, Y. Li, Q. Shen, Y. Cao, F.-Z. Li, J.-F. Wang, Y.-M. Huang, L. Deng, T. Xi, L. Ma, T. Hu, L. Li, N.-L. Liu, F. Koidl, P. Wang, Y.-A. Chen, X.-B. Wang, M. Steindorfer, G. Kirchner, C.-Y. Lu, R. Shu, R. Ursin, T. Scheidl, C.-Z. Peng, J.-Y. Wang, A. Zeilinger, and J.-W. Pan, Satellite-relayed intercontinental quantum network, *Phys. Rev. Lett.* **120**, 030501 (2018).

[13] Y.-A. Chen, Q. Zhang, T.-Y. Chen, W.-Q. Cai, S.-K. Liao, J. Zhang, K. Chen, J. Yin, J.-G. Ren, Z. Chen, S.-L. Han, Q. Yu, K. Liang, F. Zhou, X. Yuan, M.-S. Zhao, T.-Y. Wang, X. Jiang, L. Zhang, W.-Y. Liu, Y. Li, Q. Shen, Y. Cao, C.-Y. Lu, R. Shu, J.-Y. Wang, L. Li, N.-L. Liu, F. Xu, X.-B. Wang, C.-Z. Peng, and J.-W. Pan, An integrated space-to-ground quantum communication network over 4,600 kilometres, *Nature* **589**, 214 (2021).

[14] Y.-L. Tang, H.-L. Yin, Q. Zhao, H. Liu, X.-X. Sun, M.-Q. Huang, W.-J. Zhang, S.-J. Chen, L. Zhang, L.-X. You, Z. Wang, Y. Liu, C.-Y. Lu, X. Jiang, X. Ma, Q. Zhang, T.-Y. Chen, and J.-W. Pan, Measurement-device-independent quantum key distribution over untrustful metropolitan network, *Phys. Rev. X* **6**, 011024 (2016).

[15] S. K. Joshi, D. Aktas, S. Wengerowsky, M. Lončarić, S. P. Neumann, B. Liu, T. Scheidl, G. C. Lorenzo, Željko Samec, L. Kling, A. Qiu, M. Razavi, M. Stipčević, J. G. Rarity, and R. Ursin, A trusted node-free eight-user metropolitan quantum communication network, *Science Advances* **6**, eaba0959 (2020), <https://www.science.org/doi/pdf/10.1126/sciadv.aba0959>.

[16] M. Alshowkan, B. P. Williams, P. G. Evans, N. S. Rao, E. M. Simmernan, H.-H. Lu, N. B. Lingaraju, A. M. Weiner, C. E. Marvinney, Y.-Y. Pai, B. J. Lawrie, N. A. Peters, and J. M. Lukens, Reconfigurable quantum local area network over deployed fiber, *PRX Quantum* **2**, 040304 (2021).

[17] E. Y. Zhu, C. Corbari, A. Gladyshev, P. G. Kazansky, H.-K. Lo, and L. Qian, Toward a reconfigurable quantum network enabled by a broadband entangled source, *J. Opt. Soc. Am. B* **36**, B1 (2019).

[18] W. Grice, R. Bennink, D. Earl, P. Evans, T. Humble, R. Pooser, J. Schaake, and B. Williams, Multi-client quantum key distribution using wavelength division multiplexing, in *Quantum Communications and Quantum Imaging IX*, Vol. 8163, edited by R. E. Meyers, Y. Shih, and K. S. Deacon, International Society for Optics and Photonics (SPIE, 2011) pp. 89 – 95.

[19] F. Kaiser, L. A. Ngah, A. Issautier, T. Delord, D. Aktas, V. D'Auria, M. De Micheli, A. Kastberg, L. Labonté, O. Al-

ibart, A. Martin, and S. Tanzilli, Polarization entangled photon-pair source based on quantum nonlinear photonics and interferometry, *Optics Communications* **327**, 7 (2014).

[20] S. Wengerowsky, S. K. Joshi, F. Steinlechner, H. Hübel, and R. Ursin, An entanglement-based wavelength-multiplexed quantum communication network, *Nature* **564**, 225 (2018).

[21] S. Wengerowsky, S. K. Joshi, F. Steinlechner, J. R. Zichi, S. M. Dobrovolskiy, R. van der Molen, J. W. N. Los, V. Zwiller, M. A. M. Versteegh, A. Mura, D. Calonico, M. Inguscio, H. Hübel, L. Bo, T. Scheidl, A. Zeilinger, A. Xuereb, and R. Ursin, Entanglement distribution over a 96-km-long submarine optical fiber, *Proceedings of the National Academy of Sciences* **116**, 6684 (2019), <https://www.pnas.org/content/116/14/6684.full.pdf>.

[22] S. Wengerowsky, S. K. Joshi, F. Steinlechner, J. R. Zichi, B. Liu, T. Scheidl, S. M. Dobrovolskiy, R. v. d. Molen, J. W. N. Los, V. Zwiller, M. A. M. Versteegh, A. Mura, D. Calonico, M. Inguscio, A. Zeilinger, A. Xuereb, and R. Ursin, Passively stable distribution of polarisation entanglement over 192 km of deployed optical fibre, *npj Quantum Information* **6**, 5 (2020).

[23] Y. Shi, S. Moe Thar, H. S. Poh, J. A. Grieve, C. Kurt-siefer, and A. Ling, Stable polarization entanglement based quantum key distribution over a deployed metropolitan fiber, *Applied Physics Letters* **117**, 124002 (2020), <https://doi.org/10.1063/5.0021755>.

[24] K. Yoshino, T. Ochi, M. Fujiwara, M. Sasaki, and A. Tajima, Maintenance-free operation of wdm quantum key distribution system through a field fiber over 30 days, *Opt. Express* **21**, 31395 (2013).

[25] Y.-Y. Ding, H. Chen, S. Wang, D.-Y. He, Z.-Q. Yin, W. Chen, Z. Zhou, G.-C. Guo, and Z.-F. Han, Polarization variations in installed fibers and their influence on quantum key distribution systems, *Opt. Express* **25**, 27923 (2017).

[26] R. Liu, H. Yu, J. Zan, S. Gao, L. Wang, M. Xu, J. Tao, J. Liu, Q. Chen, and Y. Zhao, Analysis of polarization fluctuation in long-distance aerial fiber for qkd system design, *Optical Fiber Technology* **48**, 28 (2019).

[27] J. Chen, G. Wu, Y. Li, E. Wu, and H. Zeng, Active polarization stabilization in optical fibers suitable for quantum key distribution, *Opt. Express* **15**, 17928 (2007).

[28] G. B. Xavier, G. V. de Faria, T. F. da Silva, G. P. Temporão, and J. P. von der Weid, Active polarization control for quantum communication in long-distance optical fibers with shared telecom traffic, *Microwave and Optical Technology Letters* **53**, 2661 (2011), <https://onlinelibrary.wiley.com/doi/pdf/10.1002/mop.26320>.

[29] D.-D. Li, S. Gao, G.-C. Li, L. Xue, L.-W. Wang, C.-B. Lu, Y. Xiang, Z.-Y. Zhao, L.-C. Yan, Z.-Y. Chen, G. Yu, and J.-H. Liu, Field implementation of long-distance quantum key distribution over aerial fiber with fast polarization feedback, *Opt. Express* **26**, 22793 (2018).

[30] C. H. Bennett, G. Brassard, and N. D. Mermin, Quantum cryptography without bell's theorem, *Phys. Rev. Lett.* **68**, 557 (1992).

[31] J. Brendel, N. Gisin, W. Tittel, and H. Zbinden, Pulsed energy-time entangled twin-photon source for quantum communication, *Phys. Rev. Lett.* **82**, 2594 (1999).

[32] W. Tittel, J. Brendel, H. Zbinden, and N. Gisin, Quantum cryptography using entangled photons in energy-time bell states, *Phys. Rev. Lett.* **84**, 4737 (2000).

[33] Y.-H. Li, Z.-Y. Zhou, Z.-H. Xu, L.-X. Xu, B.-S. Shi, and G.-C. Guo, Multiplexed entangled photon-pair sources for all-fiber quantum networks, *Phys. Rev. A* **94**, 043810 (2016).

[34] J. D. Franson, Bell inequality for position and time, *Phys. Rev. Lett.* **62**, 2205 (1989).

[35] I. Marcikic, H. de Riedmatten, W. Tittel, H. Zbinden, M. Legré, and N. Gisin, Distribution of time-bin entangled qubits over 50 km of optical fiber, *Phys. Rev. Lett.* **93**, 180502 (2004).

[36] T. Inagaki, N. Matsuda, O. Tadanaga, M. Asobe, and H. Takesue, Entanglement distribution over 300 km of fiber, *Opt. Express* **21**, 23241 (2013).

[37] T. Honjo, S. W. Nam, H. Takesue, Q. Zhang, H. Kamada, Y. Nishida, O. Tadanaga, M. Asobe, B. Baek, R. Hadfield, S. Miki, M. Fujiwara, M. Sasaki, Z. Wang, K. Inoue, and Y. Yamamoto, Long-distance entanglement-based quantum key distribution over optical fiber, *Opt. Express* **16**, 19118 (2008).

[38] W.-T. Fang, Y.-H. Li, Z.-Y. Zhou, L.-X. Xu, G.-C. Guo, and B.-S. Shi, On-chip generation of time-and wavelength-division multiplexed multiple time-bin entanglement, *Opt. Express* **26**, 12912 (2018).

[39] M. D. A.D. Kersey, M.J. Marrone, Polarisation-insensitive fibre optic michelson interferometer, *Electronics Letters* **27**, 518 (1991).

[40] V. Secondi, F. Sciarrino, and F. De Martini, Quantum spin-flipping by the faraday mirror, *Phys. Rev. A* **70**, 040301 (2004).

[41] M. Martinelli, A universal compensator for polarization changes induced by birefringence on a retracing beam, *Optics Communications* **72**, 341 (1989).

[42] O. Alibart, V. D'Auria, M. D. Micheli, F. Doutre, F. Kaiser, L. Labonté, T. Lunghi, É. Picholle, and S. Tanzilli, Quantum photonics at telecom wavelengths based on lithium niobate waveguides, *Journal of Optics* **18**, 104001 (2016).

[43] D. Aktas, B. Fedrici, F. Kaiser, T. Lunghi, L. Labonté, and S. Tanzilli, Entanglement distribution over 150 km in wavelength division multiplexed channels for quantum cryptography, *Laser & Photonics Reviews* **10**, 451 (2016), <https://onlinelibrary.wiley.com/doi/pdf/10.1002/lpor.201500258>.

[44] D. Elkouss, A. Leverrier, R. Alleaume, and J. J. Boutros, Efficient reconciliation protocol for discrete-variable quantum key distribution, *2009 IEEE International Symposium on Information Theory*, 1879 (2009).

[45] X. Liu, X. Yao, R. Xue, H. Wang, H. Li, Z. Wang, L. You, X. Feng, F. Liu, K. Cui, Y. Huang, and W. Zhang, An entanglement-based quantum network based on symmetric dispersive optics quantum key distribution, *APL Photonics* **5**, 076104 (2020), <https://doi.org/10.1063/5.0002595>.

[46] N. B. Lingaraju, H.-H. Lu, S. Seshadri, D. E. Leaird, A. M. Weiner, and J. M. Lukens, Adaptive bandwidth management for entanglement distribution in quantum networks, *Optica* **8**, 329 (2021).

[47] ID Quantique SA, "ID 281 Superconducting nanowire system - Product broch (2021).

[48] X. Zhang, B. A. Bell, A. Mahendra, C. Xiong, P. H. W. Leong, and B. J. Eggleton, Integrated silicon nitride time-bin entanglement circuits, *Opt. Lett.* **43**, 3469 (2018).

[49] F. Cavaliere, J. Mattsson, and B. Smeets, The security implications of quantum cryptography and quantum computing, *Network Security* **2020**, 9 (2020).

[50] H. Takesue, K. ichi Harada, K. Tamaki, H. Fukuda, T. Tsuchizawa, T. Watanabe, K. Yamada, and S. ichi Itabashi, Long-distance entanglement-based quantum key distribution experiment using practical detectors, *Opt. Express* **18**, 16777 (2010).

[51] P. Roztocki, B. MacLellan, M. Islam, C. Reimer, B. Fischer, S. Sciara, R. Helsten, Y. Jestin, A. Cino, S. T. Chu, B. Little, D. J. Moss, M. Kues, and R. Moran-

dotti, Arbitrary phase access for stable fiber interferometers, *Laser & Photonics Reviews* **15**, 2000524 (2021), <https://onlinelibrary.wiley.com/doi/pdf/10.1002/lpor.202000524>.

[52] J.-Y. Liu, H.-J. Ding, C.-M. Zhang, S.-P. Xie, and Q. Wang, Practical phase-modulation stabilization in quantum key distribution via machine learning, *Phys. Rev. Applied* **12**, 014059 (2019).

[53] N. T. Islam, C. Cahall, A. Aragoneses, A. Lezama, J. Kim, and D. J. Gauthier, Robust and stable delay interferometers with application to  $d$ -dimensional time-frequency quantum key distribution, *Phys. Rev. Applied* **7**, 044010 (2017).

[54] X.-F. Mo, B. Zhu, Z.-F. Han, Y.-Z. Gui, and G.-C. Guo, Faraday–michelson system for quantum cryptography, *Opt. Lett.* **30**, 2632 (2005).